SCIENTIFIC REPORTS

OPEN

SUBJECT AREAS:
ENVIRONMENTAL MONITORING
POLLUTION REMEDIATION

Received
18 June 2014

Accepted
6 October 2014

Published
23 October 2014

Correspondence and requests for materials should be addressed to H.U.L. (leeho@kbsi.re.kr); Y.-S.L. (youngslee@cnu.ac.kr) or J.L. (jouhahn@kbsi.re.kr)

* These authors contributed equally to this work.

Innovative three-dimensional (3D) *eco*-TiO_2 photocatalysts for practical environmental and bio-medical applications

Hyun Uk Lee[1]*, Soon Chang Lee[2]*, Young-Chul Lee[3]*, Byoungchul Son[4], So Young Park[1], Jae Won Lee[5], You-Kwan Oh[6], Yooseok Kim[1], Saehae Choi[7], Young-Seak Lee[2] & Jouhahn Lee[1]

[1]Division of Materials Science, Korea Basic Science Institute (KBSI), Daejeon 305-333, Republic of Korea, [2]Department of Applied Chemistry and Biological Engineering, Chungnam National University, Daejeon 305-764, Republic of Korea, [3]Department of BioNano Technology, Gachon University, 1342 Seongnamdaero, Sujeong-gu, Seongnam-si, Gyeonggi-do 461-701, Republic of Korea, [4]Korea Advanced Institute of Science and Technology, Research analysis center, Daejeon 305-701, Republic of Korea, [5]Department of Energy Engineering, Dankook University, Cheonan 330-714, Republic of Korea, [6]Biomass and Waste Energy Laboratory, Korea Institute of Energy Research (KIER), Daejeon 305-343, Republic of Korea, [7]Environmental Biotechnology Research Center, KRIBB, Daejeon 305-806, Republic of Korea.

It is known that water purified by conventional TiO_2 photocatalysts may not be safe enough for drinking, due to the toxicity by tiny existence of TiO_2 nanoparticles after water treatment. We herein demonstrate a facile design of a three-dimensional (3D) TiO_2 photocatalyst structure with which both the efficiency of purification and the safety level of the final purified water can be improved and ensured, respectively. The structure, consisting of 3D sulfur-doped TiO_2 microtubes in nanotubes (*eco*-TiO_2), is suitable for both environmental and bio-medical applications. Investigation of its formation mechanism reveals that anodic aluminum oxide (AAO), owing to a spatial constraint, causes a simple, nanoparticles-to-nanotubes structural rearrangement as a template for nanotube growth. It is found that *eco*-TiO_2 can be activated under visible-light irradiation by non-metal (sulfur; S) doping, after which it shows visible-light photocatalytic activities over a range of solar energy. Importantly, an *in vitro* cytotoxicity test of well-purified water by *eco*-TiO_2 confirms that *eco*-TiO_2 satisfies the key human safety conditions.

One of the most significant environmental issues today is the potential of photocatalytic technology to provide solutions to various environmental problems faced by our society[1,2]. TiO_2 particularly, a typical photocatalyst, has various environmental applications[3–8]. For example, it is known to exhibit excellent photocatalytic behavior for decomposition of volatile organic compounds in air/water and bacterial treatments[9–13]. Practical environmental applications for TiO_2 photocatalysts require the synthesis of immobilized TiO_2 films on suitable substrates[3]. However, immobilized TiO_2 film occasionally shows lower photocatalytic activity due to surface-area diminution, limited mass diffusion, and/or the application only of UV-light photoactivity[1–3]. It is therefore necessary to improve the photocatalytic activity of TiO_2 film by optimization of several factors such as thickness, size, porosity, crystal structure, and (non-) metal doping.

Porous TiO_2 nanotubes are among the most attractive of the various TiO_2 structures, owing to their excellent and highly promising performance in a variety of fields including photocatalysis, photoelectronics, semiconducting, and others[14–18]. Generally, TiO_2 nanotubes are prepared using a hard template, for example, an anodic alumina oxide (AAO) nanochannel array architecture[15,19–23]. Recent publications indicate that highly ordered and vertically oriented nanotube arrays, such as tube-in-tube[24], tube-in-tube with a porous wall[25], and tube with a mesoporous wall[26], can be utilized in electronics, optics, sensing, advanced photocatalysis, and energy storage/conversion applications. For fabrication of those TiO_2 tubes, anodization of metallic Ti is regarded as a suitable method.

The photocatalyst should retain high activity under visible-light irradiation ($\lambda > 400$ nm) in order to effectively utilize natural sunlight and maximize photocatalysis[1]. In order to utilize the wide solar energy spectrum, many efforts have been made to narrow the band-gap of TiO_2 by doping it with nonmetals such as carbon, sulfur,

nitrogen, and fluorine[1–4]. Recently, numerous impressive TiO_2-nonmetal doping processes have been devised, especially involving the use of sulfur[10,27–29]. For example, we demonstrated that sulfur-doped TiO_2 (S-TiO_2) exhibits superior visible-light photocatalytic and antibacterial activities, as well as good recycling properties[10]. Such technology using sulfur for modification of TiO_2 can actually be used in highly efficient air/water treatment, dye-sensitized solar cells, as bactericidal agents, and for self-antifouling action[27–31].

In the present study, we created three-dimensional (3D) sulfur-doped TiO_2 microtubes in nanotubes (*eco*-TiO_2) by a structurally simple rearrangement whereby the tube structure is maintained via a nanoparticles-to-nanotubes structural change within a limited space such as the nanochannels of an AAO template. Since the first implementation of TiO_2–based photocatalysts, there has been no report on *eco*-TiO_2 synthesis by the 3D-structural approach. Also, the previous research on photocatalytic TiO_2 focused only on final air/water purification or treatment[1–5], which were not be directly relevant to the reuse of purified water by photocatalysts, indicating no available data whether the treated water is safe while contacting human interface, although an important factor involved in water purification systems is the reuse of treated water by photocatalytic applications. In the present study, we modeled global *eco*-TiO_2 materials and monitored by-products of treated water in an *in vitro* cytotoxicity assay measuring the level of water purification after photocatalytic treatment. Further, we studied the detailed *eco*-TiO_2 formation mechanism and its fundamental photochemical properties. Our findings indicated that *eco*-TiO_2 shows an efficient water-treatment performance together with an economic dividend.

Results

Fig. 1 and S1 show that the 3D TiO_2 microtubes in nanotubes (3D-TiO_2) covered the entire substrate surface. The enlarged field-emission scanning electron microscopy (FE-SEM) images clearly show the numerous 3D-TiO_2 arrays to be both uniform and compact, with lengths of at least several micrometers (~10 μm) (Fig. 1a) and outer tube diameters of a few micrometers (~1 μm) (Figs. 1a and 1b). The inter-nanotubes showed a coarse lateral profile (Fig. 1b, inset) and had a larger contact surface area than conventional structures, which structural morphologies make them good candidates for photocatalytic applications. On high-resolution transmission electron microscopy (HR-TEM) and scanning transmission electron microscopy (STEM) images of the as-grown and *eco*-TiO_2 samples (Figs. 1c, 1d, and S1), the *eco*-TiO_2 structures showed uniform diameters throughout their lengths, and the TiO_2 microtubes revealed their nanotube-like 3D-structural composition (Fig. 1c). In a detailed chemical analysis of the arrays by energy-dispersive X-ray spectroscopy (EDS) (Fig. S2, overlay), the *eco*-TiO_2 nanostructures were composed of Ti, S and O (the Cu and Al signals were caused by the TEM grid and AAO template).

The corresponding X-ray diffraction (XRD) patterns, as recorded from the as-grown and annealed *eco*-TiO_2 samples, are shown in Fig. 2. They evidence the fact that whereas the titanate phase of the 3D-TiO_2 samples (JCPDS card No. 00-047-0124) was dominant before annealing, after annealing at 350°C for 1 h, it was transformed into anatase TiO_2 (JCPDS card No. 02–0406) with higher photocatalytic activity. The XRD patterns also clearly indicate that the diffraction peaks of the *eco*-TiO_2 samples were shifted to higher diffraction angles (~0.2°) relative to those of the other samples. This implies that, after our method's high-energy treatment, an oxygen atom in TiO_2 in the *eco*-TiO_2 lattice was replaced by a sulfur atom[10].

For further investigation of the chemical states of the *eco*-TiO_2 samples, high-resolution X-ray photoelectron spectroscopy (HR-XPS) measurements were carried out. In Fig. 3's HR-XPS spectra of the S2p region of the *eco*-TiO_2 samples, it is apparent that the S2p peaks around 167.4 eV and 168.5 eV were shifted negatively by 0.5 eV relative to other research group's reported standard binding energy of sulfur in pure SO_3^{2-} (S^{4+}, 167.7 eV) and SO_4^{2-} (S^{6+}, 168.7 eV)[32–34]. All of the sulfur atoms were in the S^{2-} state, with a peak at approximately 160–163 eV[33,34]. This finding corresponds to the Ti–S bond formed when some of the oxygen atoms in the TiO_2 lattice were replaced by sulfur atoms. This leads to the large formation energy required for Ti–S bonds instead of Ti–O bonds. Thus, the replacement of Ti^{4+} by S^{4+}/S^{6+} is chemically more favorable than that of O^{2-} by S^{2-}, and consequently, Ti–O–S (or Ti-S-O) bonds are formed[10,32–34]. Although anionic sulfur (S^{2-}) doping was reported as a difficulty to be performed because the ionic radius of S^{2-} (1.7 Å) is significantly larger than that of O^{2-} (1.22 Å)[10,32] but it was

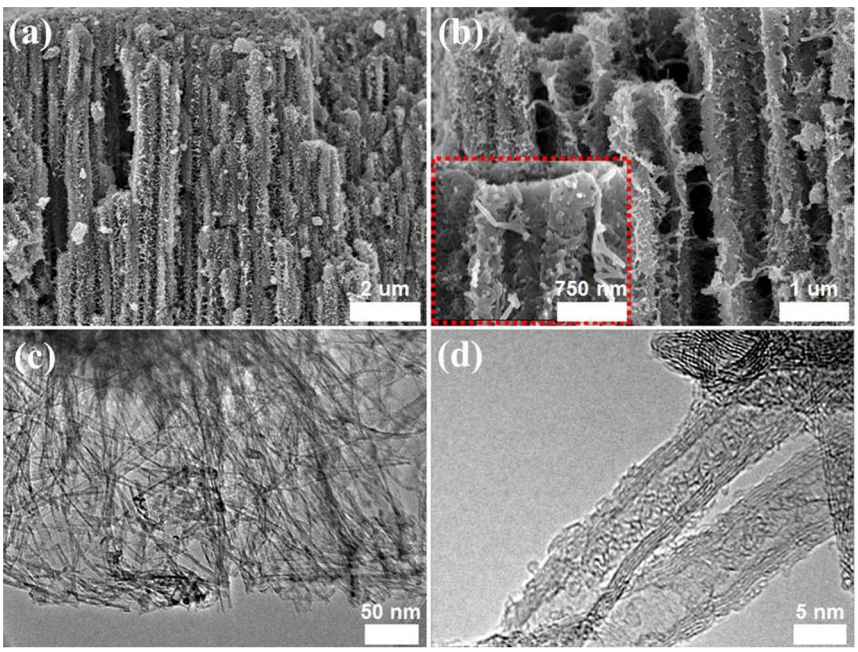

Figure 1 | (a and b) FE-SEM in which dotted box shows a partially enlarged image of (b) and (c and d) TEM images of the 3D sulfur (S)-doped TiO_2 microtubes in nanotubes (*eco*-TiO_2) samples.

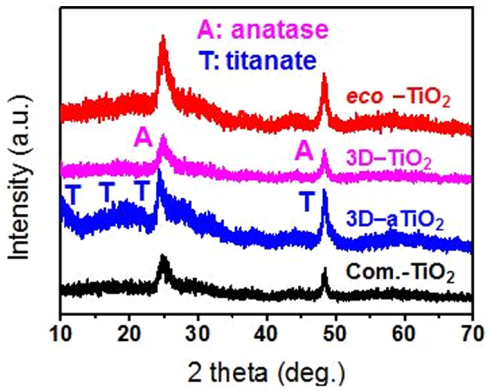

Figure 2 | XRD patterns of commercial TiO_2 (Com.-TiO_2), as-grown 3D-TiO_2 (3D-aTiO_2), 3D-TiO_2, and *eco*-TiO_2 samples. The anatase and titanate peaks are identified as A and T respectively.

revealed by XPS spectra (Fig. 3b) where the inset exhibited both S^{4+}/S^{6+} at ~168.0 eV and S^{2-} species at ~162.0 eV in *eco*-TiO_2 lattices[10,34,35], confirming that the Ti-S bonds were formed. Note that that as-prepared *eco*-TiO_2 sample was washed with deionized water and 1 M HCl solution several times to remove the surface-adsorbed SO_4^{2-} or SO_3^{2-} species.

Our simple structural rearrangement is required for the formation of *eco*-TiO_2 photocatalysts, owing to the special 3D nanostructure (Fig. 4). First, using our method, TiO_2 nanoparticles, which will be changed into TiO_2 nanotubes within the nanochannel arrays of the AAO membrane (anodisc 47, Whatman®), are generated. To achieve 3D-TiO_2 of high surface area, surfactant solutions (25 wt% solutions) are first coated onto the internal wall surfaces of the AAO template. This allows the formation of TiO_2 nanoparticles (the corresponding synthetic results are available in previously published research[15,19–23], specifically by the filling of the titanium isopropoxide (TIP) precursor in the AAO nanochannel arrays with a sol-gel reaction. The TiO_2 nanoparticle/AAO composites are then dried for 24 h at 100°C in air. Special attention should be paid to the filling of the AAO nanochannels, as, if the surfactant solution is fully filled within the nanochannel arrays, there would be no space for the precursor. The Ti precursor, therefore, should be filled only after removing the surfactant to some extent by vacuum filtration. Via a simple alkaline hydrothermal reaction, the formed nanoparticles are transformed into titanate nanotubes within the limited space of the nanochannels, AAO providing the template for nanotube growth[14–20]. The general mechanism of titanate nanotube formation is as follows: a nanosheet-type structure of sodium titanate ($Na_2Ti_3O_7$) is formed[16–24] and then, after exfoliation, is folded into a nanotube; it grows in the axis direction and is protonated via HCl rinsing ($H_2Ti_3O_7$)[14–20]; 3D-TiO_2 is formed by the effect of the nanochannel array pattern of AAO; pure anatase 3D-TiO_2 and *eco*-TiO_2 are formed by annealing and repetitive ultrasound irradiation/annealing processes[10,12]. Notably, we found that the as-grown 3D-TiO_2 at 300–450°C prevented the formation of brookite and rutile titania. This implies that by controlling the annealing temperature, the titanate of the as-grown *eco*-TiO_2 was successfully crystallized to an anatase phase.

Additionally, the 3D-TiO_2 sample showed a broad photoluminescence (PL) emission peak located around 528.9 nm (Fig. 5a). However, for the *eco*-TiO_2 sample, broad visible PL bands centered at 602.1 nm were observed. It can be seen from Figure 5a that the PL intensity of the 3D-TiO_2 was much higher than in the spectra for the *eco*-TiO_2 sample, indicating that non-metal (S) doping can effectively inhibit the recombination of excited electrons and holes[10]. This is the reason for the excited electron transference from the valence band to the new, S-doping-induced defect levels existing near the conduction band minimum, which also decreased the PL intensity. Closer inspection of Fig. 5a reveals a 73.2 nm (*eco*-TiO_2) shift of the emission peaks toward longer wavelengths when nonmetals were doped into the TiO_2 nanotubes. The emission signal at 602.1 nm might have originated from the charge-transfer transition from the oxygen vacancies to the new energy levels caused by non-metal (S) doping. Fig. 5b shows the reflectance spectra of the *eco*-TiO_2. Clearly, compared with the TiO_2 nanotubes, the action region of the *eco*-TiO_2 extended significantly into the visible-light region. The corresponding action spectra strongly suggest that *eco*-TiO_2 can be activated by visible-light irradiation. In addition, the photocurrent density was increased in the order of *eco*-TiO_2 > S-TiO_2 > 3D-TiO_2 at all $\lambda <$ 400 nm, $\lambda >$ 400 nm, and $\lambda >$ 600 nm. Particularly, the photocurrent density ($\mu A/cm^2$) with 16–20 of *eco*-TiO_2 was higher than that with 12–18 of S-TiO_2 (Fig. S3). It is associated with three-dimensional (3D) structure, corresponding to the PL quenching data (Fig. 3a). Based on the shift of absorbance peak to visible light regions in sulfur doped TiO_2 (*eco*-TiO_2), it is indicated that sulfur ions (S^{2-} and S^{6+}) are incorporated and subsequently changed into crystal and electronic structures in *eco*-TiO_2 lattices, corresponding to the rearrangement of *eco*-TiO_2 surfaces in XPS spectra, suggesting that *eco*-TiO_2 photocatalysts are strongly activated on wide visible light ranges[10,34,35].

In addition to the confirmation of efficient charge separation in electron-hole (e^-/h^+) pairs, evidenced by photocurrent and PL quenching data, the delay in charge recombination in *eco*-TiO_2 can be explained with the enhanced photocurrent. Harsh condition, i.e., H_2SO_4 treated with sonication, for sulfur (S) doping might increase surface oxygen vacancies and defects, leading to the suppression of the recombination of the photoinduced electrons and holes by capturing the photoinduced electrons[36,37]. Furthermore, in case of sulfur (S)-doped TiO_2 nanoparticles, the abundant sulfur (S)-functional groups on the surface of TiO_2 nanoparticles can facilely trap electrons (e-) in the charge recombination (e^-/h^+) pairs, resulting in

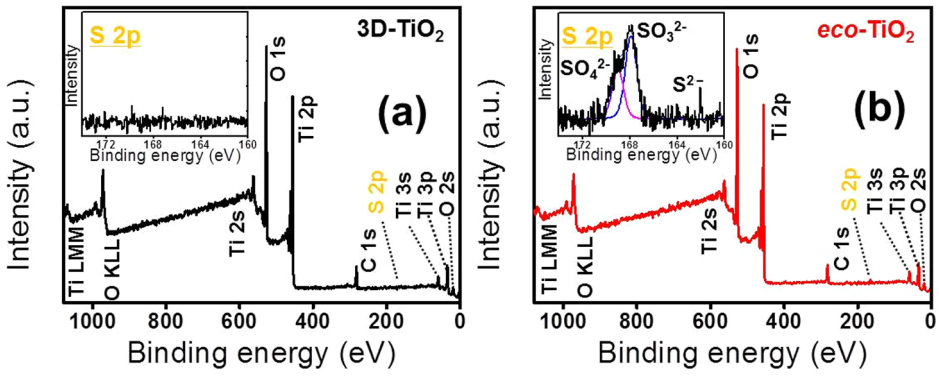

Figure 3 | High-resolution X-ray photoelectron spectra (HR-XPS) of (a) 3D-TiO_2 and (b) *eco*-TiO_2 where the inset in (b) indicates the deconvolution fitting of the S 2p of *eco*-TiO_2.

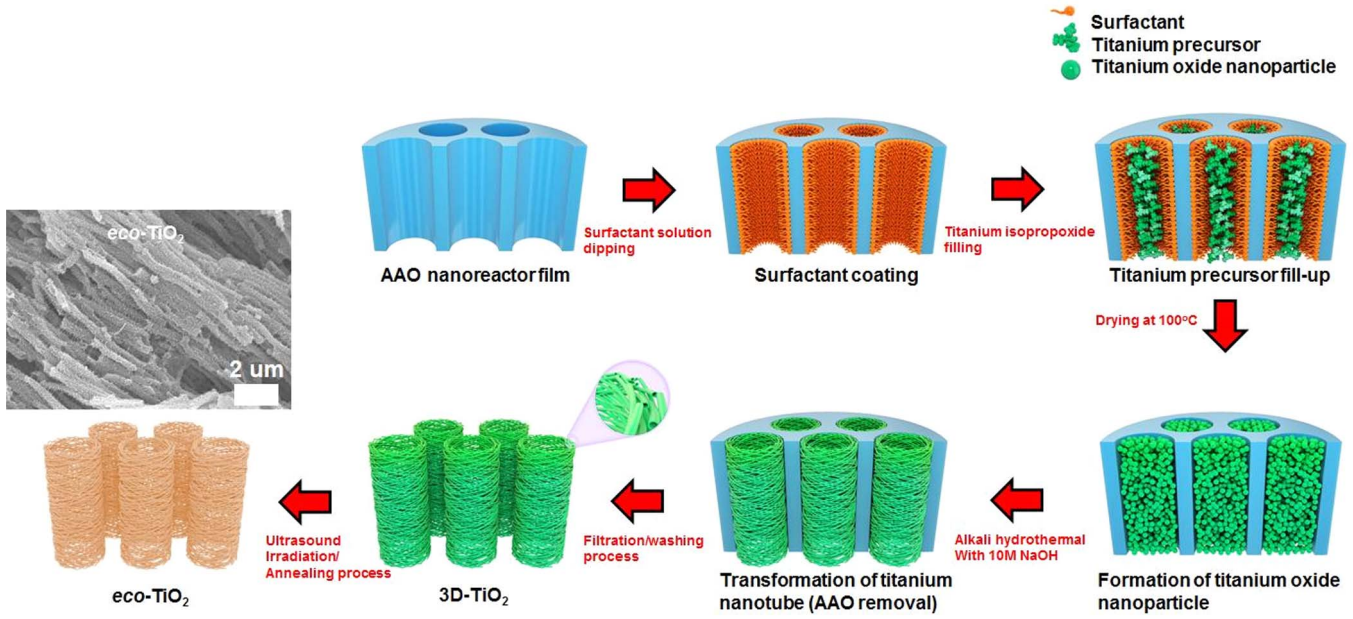

Figure 4 | **Possible mechanism for formation of *eco*-TiO_2 with anatase crystalline while retaining large surface area.**

improvement of the photocatalytic efficiencies of *eco*-TiO_2[38]. Such efforts to sink electrons neighboring microenvironment from the photogenerated charge carriers promoted to decrease in the charge recombination of TiO_2 photocatlysts[39].

For provision of information on free radicals in environmental and biological systems, 5,5-dimethyl-1-pyrroline *N*-oxide (DMPO) is frequently used in electron spin resonance (ESR) spin-trapping experiments. In the present study, detection of ·OH radicals by DMPO spin trapping for *eco*-TiO_2 samples under UV light (λ = 365 nm, 5 min irradiation) in a PBS buffer solution was investigated[30,31] (Fig. 6). The characteristic 1:2:2:1 quartet signal of a DMPO-·OH adduct appeared in both TiO_2 samples[31]. Significantly, the ESR signal intensity of the *eco*-TiO_2 was strongly enhanced, growing to approximately 3.7 times that of 3D-TiO_2. This is attributable to the facilitation of electron transference from the valence band to the conduction band, which results in the reaction of valence band holes (h^+_{vb}) with OH^- ions, producing ·OH radicals[30,31]. Importantly, the visible-light-induced ESR signal patterns in the *eco*-TiO_2 in the PBS buffer solution ($\lambda > 400$ nm, 5 min irradiation) showed intrinsic signals corresponding to S-doped TiO_2, while no signals were detected for those in the 3D-TiO_2.

Next, the photocatalytic activities of the *eco*-TiO_2 samples were evaluated by measuring the decomposition rate of Rhodamine B (Rho B) solutions under UV- and visible-light irradiation (Fig. 7). Without a photocatalyst, Rho B was hardly degraded under UV- and visible-light irradiation: the dye-color removal was only 1% under 70 min UV-light irradiation, and a paltry 0.4% under 70 min visible-light irradiation. Contrastingly, with the *eco*-TiO_2 photocatalysts, 100% color removal was achieved under the identical irradiation conditions. The superior UV-light activity of the *eco*-TiO_2 samples can be ascribed to their higher surface areas and lower electron-hole pair numbers (Fig. 5 and Table S1) because the measured BET surface area (m^2/g), pore diameter (nm), and pore volume (cm^3/g) of *eco*-TiO_2 were 276.2, 1.85, and 0.13 whose physicochemical properties are enhanced values, compared to 276.2, 1.85, and 0.13 of equivalent 3D-TiO_2. As a reference, although pore diameter (nm) of S-TiO_2, which was prepared sulfur doped commercial TiO_2 using same method of *eco*-TiO_2, showed highest 5.01 nm but BET surface area of that was significantly low value (51.4 m^2/g) with approximately 5-fold for that of *eco*-TiO_2. Even so, the TiO_2 nanotubes showed very poor photocatalytic activities under visible-light irradiation. The highest degradation rate for *eco*-TiO_2 ($[k]$ = 3.3814 h^{-1}) was 10 times faster than that of 3D-TiO_2 ($[k]$ = 0.3278 h^{-1}). In Fig. S4, other dyes such as MB and RB 5 were degraded by *eco*-TiO_2 with its relating by-products measurement as total organic carbon (TOC) results, showing a similar degradation

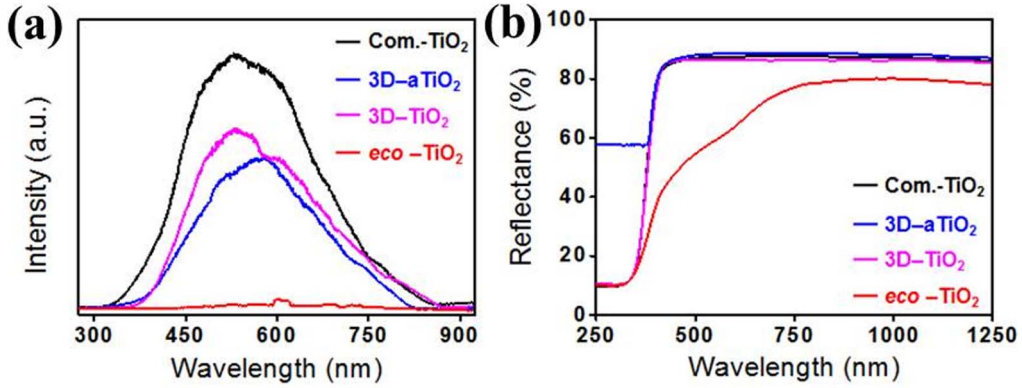

Figure 5 | (a) Photoluminescence (PL) and (b) UV-Vis-NIR reflectance spectra of commercial TiO_2 (Com.-TiO_2), as-grown 3D-TiO_2 (3D-aTiO_2), 3D-TiO_2, and eco-TiO_2 samples.

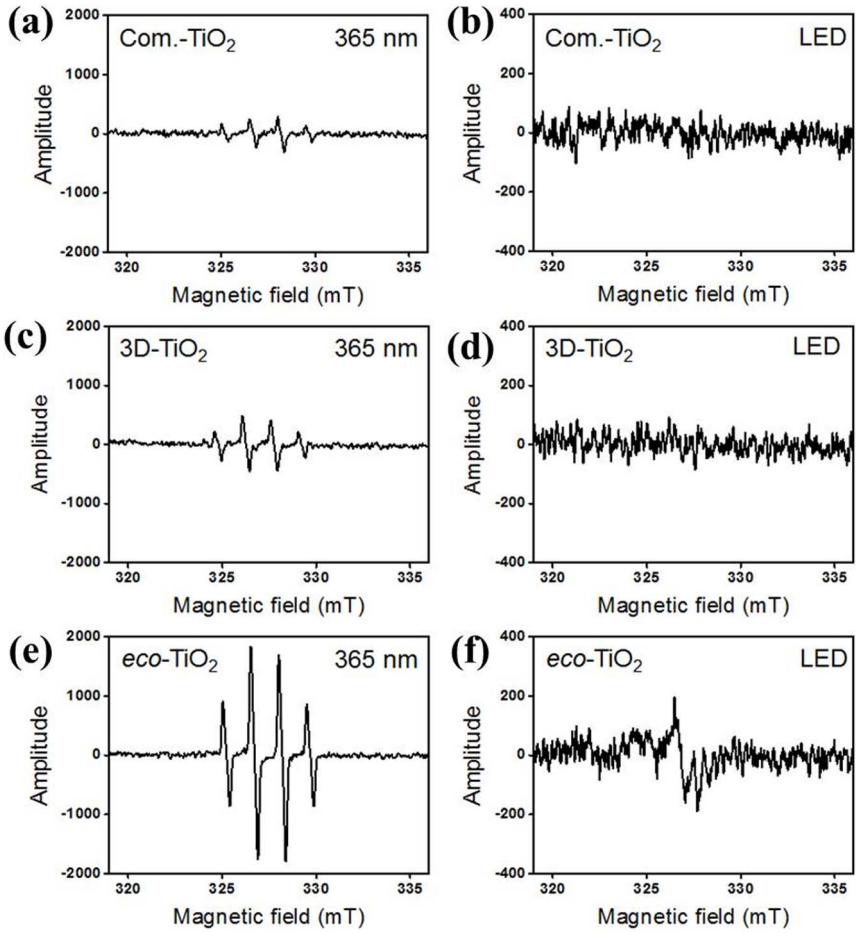

Figure 6 | ESR spectra of (a and b) commercial TiO_2 (Com.-TiO_2), (c and d) 3D-TiO_2, and (e and f) *eco*-TiO_2 samples.

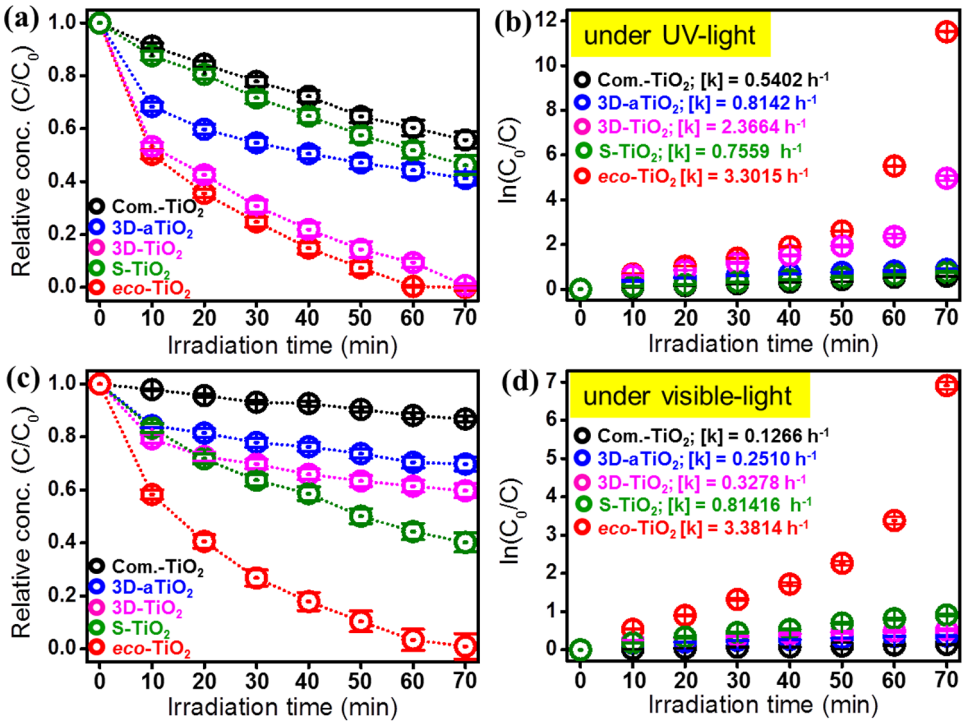

Figure 7 | Decomposition results of Rho B by commercial TiO_2 (Com.-TiO_2), as-grown 3D-TiO_2 (3D-aTiO_2), S-TiO_2, 3D-TiO_2, and *eco*-TiO_2 samples under (a and b) UV and (c and d) visible irradiation.

pattern. In order to avoid the self-photosentization of dyes, spectra scans of phenol (Ph) degradation by Com.-TiO_2, 3D-aTiO_2, 3D-TiO_2, S-TiO_2, and *eco*-TiO_2 were observed (Fig. S5a–e) and it resulted in the apparent rate constants ([*k*] = 0.009, 0.014, 0.048, 0.298, and 1.643 h^{-1}) (Fig. S5f), showing *eco*-TiO_2 possesses an efficient photocatalytic activity. As noted above, S doping might possibly have generated an intermediate energy level above the valence band of TiO_2, thereby narrowing the band-gap for induction of visible-light absorption. The TiO_2 nanotubes exhibited almost no visible-light activity, owing to the approximately 2.8–3.0 eV band-gap energy of the general TiO_2 photocatalyst[1–5]. After S atoms were doped into the TiO_2 nanotubes, the visible-light photocatalytic activities of the as-prepared samples increased greatly (Fig. S6). As increase in sulfur doing concentration in 3D-TiO_2 (i.e., 0.4%, 0.8%, and 1.2%) (Fig. S7a), the bandgap energy (eV) was decreased to 2.26, 2.21, and 2.02, respectively. Proportionally, the Rho B degradation efficiencies were slightly enhanced (Fig. S7b), although BET surface area of 0.8% S 3D-TiO_2 was higher (271.4 m^2/g) than 1.2% S 3D-TiO_2 (i.e., *eco*-TiO_2), showing similar values of pore diameter (nm) and pore volume (cm^3/g) in respective 0.8% S 3D-TiO_2 and 1.2% S 3D-TiO_2 (i.e., *eco*-TiO_2) (Table S2). The quantities of evolved CO_2 during the photocatalytic reaction of Rho B with the TiO_2 photocatalysts under visible-light irradiation are plotted in Fig. 8a. As is apparent, the evolved CO_2 increased gradually as the photocatalytic reaction progressed. After 70 min visible-light irradiation, the quantity of the evolved CO_2 for *eco*-TiO_2 (0.115 mmol) was four times higher than that for 3D-TiO_2 (0.031 mmol). These results reflect the high degree of mineralization achieved for Rho B. The length of one cycle was 70 min (visible-light irradiation time); after each interval, the decolorization was measured (Fig. 8b). After 15 repetitions, the photocatalytic conversion ratio of Rho B by *eco*-TiO_2 remained at about 92.6%. The decrease in the photocatalytic conversion ratio after every cycle was probably caused by the tiny loss of the *eco*-TiO_2 photocatalyst. However, it is clear that the removal efficiency of organic contaminants using *eco*-TiO_2 remained approximately constant even after 15 cycles. Undoubtedly, in this case, *eco*-TiO_2 exhibited excellent photocatalytic stability.

The previous research on the photocatalytic activities of metal-oxide materials focused only on final water purification under UV- and visible-light irradiation, which is not directly related to the reuse of ventilated water with a product for dye-contaminated water[1–5]. Therefore, in the present research, we carried out an *in vitro* cytotoxicity test for monitoring of by-products in Rho B treated water and measurement of the available level of water. In the results, we found that the purified water by *eco*-TiO_2 was safe enough for human cells. In an evaluation of the cytotoxicity of purified water by *eco*-TiO_2 under visible-light irradiation, the relative viabilities of CHO-K1 (ovary, Chinese hamster), COS-7 (kidney, African green monkey), and HepG2 (hepatocellular carcinoma, human) cells exposed to purified water were measured using the 3-[4,5-dimethylthiazol-2-yl]-2,5 diphenyl tetrazolium bromide (MTT) assay (Fig. 9). Fig. 9 shows the cell viability after incubation for 12, 24, and 72 h with the purified-water solution at purification degrees ranging from 0 to 100%. Below the purification degree of 98%, the cell viabilities were decreased or reduced to zero by azo dye contaminants or other chemicals noxious to organs in the water solution. After 24 h of incubation at the purification degree of 98%, the cell viability increased less than 16–18% (cellular viability: 96.2% ± 5.1% for CHO-K1, 95.5% ± 4.5% for HepG2, 94.8% ± 6.2% for COS-7; mean ± SEM, N = 5; probability value $p < 0.005$). These observations clearly show that over 12, 24 and 72 h periods, the purified water (at purification degrees of up to 98%) did not exert any cytotoxic effects on the cells, which is one of the key safety criteria. Importantly, at purification degrees typically used in nontoxic cell cultivation (>98%), the cytotoxicity of purified water was found to be marginal. Additionally, it was confirmed for the similar cytotoxicity results, after 24 h incubation, for other dyes treatment by *eco*-TiO_2, resulting in (cellular viability: 89.0% ± 9.0%/92.0% ± 8.0% for CHO-K1, 91.0% ± 8.0%/90.0% ± 8.0% for COS-7; mean ± SEM, N = 5; probability value $p < 0.005$) for 98% of MB- and RB 5 purified water, respectively (Fig. S8). Therefore, treatment of dye-contaminated water by *eco*-TiO_2, capable of greater-than-98% removal efficiency, can be considered to be an efficient non-cytotoxic clean-up method.

Discussion

We developed a photocatalyst, *eco*-TiO_2, for purification of organic-pollutant-contaminated water that is suitable for human consumption. The *eco*-TiO_2 was synthesized via a structural rearrangement entailing the changing of nanoparticles to nanotubes within an AAO template that provided a limited space (nanochannels) for TiO_2 nanotube growth. *Eco*-TiO_2 was designed to achieve higher surface areas and lowered electron-hole pairs with uniform diameters in a 3D architecture. The as-prepared *eco*-TiO_2 exhibited broad visible PL bands centered at 634.59 nm after S atoms were doped into the TiO_2 nanotubes. These results clearly indicated that the photocatalytic activities of the *eco*-TiO_2 under visible light were markedly superior to those of TiO_2. Using *eco*-TiO_2, the degradation rate of the dye solution under 70 min visible-light irradiation was 100%. And as for the practical findings, the cellular viabilities of CHO-K1, HepG2, and COS-7 after 12, 24, and 72 h incubation with water solution 98% purified by *eco*-TiO_2 were as high as 96%, indicating no cytotoxicity. In terms of mitigating the impacts of environmental pollution, *eco*-TiO_2 offers a great potential for reduction of water-contamination levels by acting as an effective photocatalyst in practical bio-medical applications.

Methods

Synthesis of 3D TiO_2 microtubes in nanotubes. All of the reagents were of analytical grade (Sigma Aldrich, MO, USA), and were used without further purification.

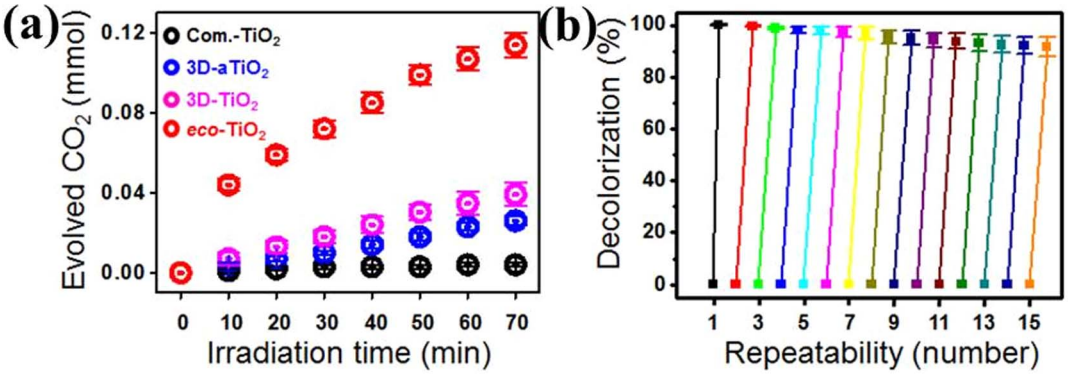

Figure 8 | (a) Evolved CO_2 of commercial TiO_2 (Com.-TiO_2), as-grown 3D-TiO_2 (3D-aTiO_2), 3D-TiO_2, and *eco*-TiO_2 samples under visible irradiation, and (b) recycling results of the *eco*-TiO_2 in decolorization for Rho B solution.

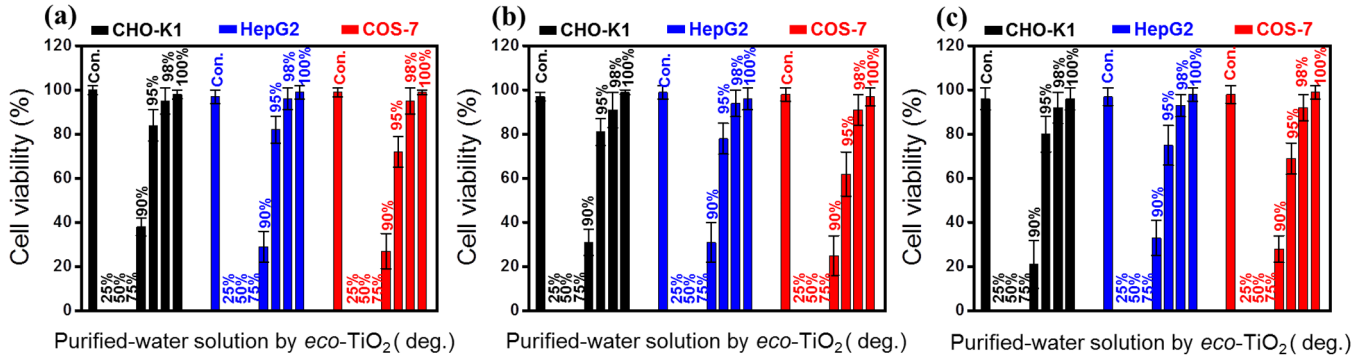

Figure 9 | Cytotoxicity studies of Rho B purified water treatment (degree of %) by *eco*-TiO_2 photocatalysts under visible-light irradiation after 12 h (a), 24 h (b), and 72 h (c) cell incubation. To evaluate the cytotoxicity of purified water by *eco*-TiO_2 photocatalysts under visible-light irradiation, the relative viabilities of CHO-K1 (ovary, Chinese hamster), COS-7 (kidney, African green monkey), and HepG2 (hepatocellular carcinoma, human) cells exposed to purified water were measured using the MTT assay. The data is presented as mean ± SE of five replicates.

Ultrapure water (18.2 MΩ/cm, DI water) from a Milli-Q ultrapure system was used in this study. In the typical synthesis, an AAO (Whatman® anodic 47, Germany) template was filled with 20 mg of a hexadecyltrimethylammonium chloride surfactant solution ($C_{19}H_{42}ClN$, molecular weight: 320) and 30 mg of a titanium isopropoxide precursor solution at 100°C before drying. Thereafter, the template was subjected to an alkaline hydrothermal reaction for 24 h at 120°C in a 10 M sodium hydroxide solution and washed several times with DI water. It was then rinsed with a 0.1 M hydrochloric acid solution and dried in vacuum for 12 h at 60°C.

Synthesis of *eco*-TiO_2. *Eco*-TiO_2 was prepared as follows. The obtained 3D-TiO_2 microtubes with nanotubes were dispersed in 900 mL of 0.1–1.0 M sulfuric acid (H_2SO_4) solution, to which 100 mL of a hydrogen peroxide (H_2O_2) solution was added dropwise with vigorous stirring for 5 min at room temperature (RT). Ultrasound irradiation was just applied for 40 min, with the electrical energy input maintained at 100 W/cm^2. The reddish-orange-colored TiO_2 powder was filtered, washed three times with DI water, and finally dried under air at RT. An *eco*-TiO_2 was then calcined up to 623 K in air.

Characterization. The crystalline structures of the *eco*-TiO_2 samples were investigated by reference to the XRD (Rigaku RDA-cA X-ray diffractometer, Japan) patterns obtained using Cu Kα radiation passed through a nickel filter. The morphology and size distribution of the *eco*-TiO_2 particles were recorded by FE-SEM (Hitachi, S-4700, Japan) and HRTEM (JEOL, JEM 2200, Japan). Preparatory to the analyses, the samples were placed onto the surfaces of copper grids and dried under ambient conditions. The Brunauer–Emmett–Teller (BET) surface areas, pore volumes, and pore diameters of the *eco*-TiO_2 particles were determined using a BET analyzer (Micromeritics ASAP 2020, USA). HR-XPS carried out using monochromatic Al Kα X-ray radiation (hν = 1486.6 eV) with a power of 120 W (Kratos Analytical, AXIS Nova, UK) was utilized to investigate the samples' surface properties. The shift in the binding energy due to relative surface charging was corrected with reference to an internal standard, namely the C1s level at 284.6 eV. A He-Cd laser (Kimmon, 1 K, Japan) of 325 nm wavelength and a power of 50 mW was utilized as an excitation source for PL measurements carried out using a spectrograph (f = 0.5 m, Acton Research Co., Spectrograph 500i, USA) with an intensified charge-coupled device (CCD; PI-MAX3, Princeton Instruments, IRY1024, USA). For free radical detection by 5,5-dimethyl-1-pyrroline *N*-oxide (DMPO, 0.3 M in PBS buffer at pH 7.2, Sigma-Aldrich, USA) spin trap agent, an aliquot of as-prepared samples (100 μL of 5 mg TiO_2 sample mixed with 300 μL DMPO solution) was filled into a capillary tube and directly irradiated with a UV (λ = 365 nm) or LED light (>400 nm) source for 5 min, after which the spectra were recorded by ESR spectrometry (JES-FA200, JEOL, Japan; center field: 327 mT; powder: 1 mW; amplitude: 5.0 × 100; modulation width: 0.4 × 1; sweep width: 1 × 10; sweep time: 30 s)[40,41]. For the photocurrent density (μA/cm^2) measurement, it was prepared with photo-electrodes by screen printing of each TiO_2 photocatalysts onto fluoride doped tin oxide-coated (FTO) glass substrate (1 × 1 inch^2)[43,44]. KI_3 solution (0.5 M) was used as an electrolyte. It was assembled the two glass (working electrode acting as photoanode-TiO_2 on FTO, and reference electrode-carbon black on FTO) plates with coated sides together, but offset so that uncoated glass extends beyond the sandwich[42-44]. Add a drop of electrolyte solution to opposite edges of the plate. Capillary action will cause the electrolyte solution to travel between the two plates. After, it was connected a multimeter (Agilent 34420A, Agilent Technologies, USA) using an alligator clip to each plate. The photocurrent was observed for each switch-on/off event by using a Xenon lamp (450 W) with a 400–600 nm cut-off filter.

Measurement of photocatalytic and antibacterial activities. The photocatalytic degradations of phenol (Ph; 3.0 mg/L, Aldrich, USA), Reactive black 5 (RB 5; 3 mg/L, Aldrich, USA), Rhodamine B (Rho B; 3 mg/L, Sigma-Aldrich, USA), and Methylene blue (MB; RB 5; 3 mg/L, Aldrich, USA) solutions by catalyst samples (0.5 g/L) were carried out under UV (source: 4 W, 365 nm, VSLAB VL-4CL, Korea) and visible-light (source: 150 W Xe lamp, λ > 420 nm, SCHOTT, USA) irradiation, and the absorbance of the solutions was measured using a UV-Vis-NIR spectrophotometer (Varian, Cary 5000, Australia) in the wavelength region 200–800 nm. The concentrations of Ph, RB 5, Rho B and MB in the solutions after photoirradiation were measured from the absorbance peak intensities of the solutions at 270, 598, 555 and 664 nm, respectively[10,12,45]. Total organic carbon (TOC) of the solution was also determined by a Shimadzu TOC-V analyzer. Light source was positioned at 15 cm height from the experimental desk. The changes in the concentration of the dye solution [$\ln(C_0/C) = kt$, where k is the apparent reaction rate constant, and C_0 and C are the initial and reaction concentrations, respectively, of Rho B] with reaction time also were investigated for all of the samples[10]. To demonstrate the stability of the photocatalysts, *eco*-TiO_2 was recycled for testing of other photocatalytic activities. The recycling tests evaluating the photocatalytic activity of *eco*-TiO_2 were performed after washing the samples three times with DI water and drying them in an oven for 6 h after each cycle[10,12]. Evolved CO_2 was analyzed with a TM IGC120-MB gas chromatograph equipped with a Q column. Additionally, an action-spectrum analysis of the photocatalytic reactions was carried out under monochromatic light irradiation from a JASCO CRM-FD diffraction-grating-type illuminator.

***In vitro* cytotoxicity test of purified water using *eco*-TiO_2.** The cytotoxicities of the samples were evaluated by a MTT assay[46]. Briefly, CHO-K1 (ovary, Chinese hamster), HepG2 (hepatocellular liver carcinoma, human), and COS-7 (kidney, African green monkey) cells were seeded in a 96-well plate at a density of 8 × 10^3 cells per well and cultured in a humidified incubator at 37°C for 24 and 72 h under a 5% CO_2 atmosphere in Dulbecco's modified Eagle's medium (DMEM) and/or Roswell Park Memorial Institute (RPMI)-1640 supplemented with 10% FBS and 1% penicillin antibiotics. The DMEM and/or RPMI-1640 media were used to purify water samples (to 0, 25, 50, 75, 90, 95, 98, and 100% degrees) using *eco*-TiO_2 photocatalysts, after which they were incubated for 24 and 72 h. Then, 20 μL of 0.2 mg/mL MTT solution in medium was added to each well and incubated at 37°C for 2 h. Finally, the optical density (OD) was measured at 490 nm with an absorbance microplate reader (EMax microplate reader, Bucher Biotec AG, Basel, Switzerland).

In the measurements of the photocatalytic activities for the antimicrobial and following cytotoxicity tests, the data were averaged and expressed as mean ± standard deviations (SE). Each test was repeated up to four times. A statistical analysis was performed by analysis of variance (ANOVA); p-values less than 0.05 were considered significant.

1. Kubacka, A., Fernandez-García, M. & Colon, G. Advanced nanoarchitectures for solar photocatalytic applications. *Chem. Rev.* **112**, 1555–1614 (2012).
2. Chen, H., Nanayakkara, C. E. & Grassian, V. H. Titanium dioxide photocatalysis in atmospheric chemistry. *Chem. Rev.* **112**, 5919–5948 (2012).
3. Chen, X. & Mao, S. S. Titanium dioxide nanomaterials: synthesis, properties, modifications, and applications. *Chem. Rev.* **107**, 2891–2959 (2007).
4. Tong, H. *et al.* Nano-photocatalytic materials: possibilities and challenges. *Adv. Mater.* **24**, 229–251 (2012).
5. Kisch, H. Semiconductor photocatalysis-mechanistic and synthetic aspects. *Angew. Chem.-Int. Edit.* **52**, 812–847 (2013).
6. Albu, S. P., Ghicov, A., Macak, J. M., Hahn, R. & Schmuki, P. Self-organized, free-standing TiO_2 nanotube membrane for flow-through photocatalytic applications. *Nano Lett.* **7**, 1286–1289 (2007).
7. Wang, X., Li, Z., Shi, J. & Yu, Y. One-dimensional titanium dioxide nanomaterials: nanowires, nanorods, and nanobelts. *Chem. Rev.* DOI: 10.1021/cr400633s (2014).
8. Xiong, Z. & Zhao, X. S. Nitrogen-doped titanate-anatase core–shell nanobelts with exposed {101} anatase facets and enhanced visible light photocatalytic activity. *J. Am. Chem. Soc.* **134**, 5754–5757 (2012).

9. Li, Y., Zhang, W., Niu, J. & Chen, Y. Mechanism of photogenerated reactive oxygen species and correlation with the antibacterial properties of engineered metal-oxide nanoparticles. *ACS Nano* **6**, 5164–5173 (2012).
10. Lee, H. U. *et al*. Highly visible-light active nanoporous TiO_2 photocatalysts for efficient solar photocatalytic applications. *Appl. Catal. B-Environ.* **129**, 106–113 (2013).
11. Tong, T. *et al*. Effects of material morphology on the phototoxicity of nano-TiO_2 to bacteria. *Environ. Sci. Technol.* **47**, 12486–12495 (2013).
12. Lee, H. U. *et al*. Influence of visible-light irradiation on physicochemical and photocatalytic properties of nitrogen-doped three-dimensional (3D) titanium dioxide. *J. Hazard. Mater.* **258**, 10–18 (2013).
13. Kamegawa, T., Shimizu, Y. & Yamashita, H. Superhydrophobic surfaces with photocatalytic self-cleaning properties by nanocomposite coating of TiO_2 and polytetrafluoroethylene. *Adv. Mater.* **24**, 3697–3700 (2012).
14. Wang, K., Wei, M., Morris, M. A., Zhou, H. & Holmes, J. D. Mesoporous titania nanotubes: their preparation and application as electrode materials for rechargeable lithium batteries. *Adv. Mater.* **19**, 3016–3020 (2007).
15. Zheng, Q. *et al*. Self-organized TiO_2 nanotube array sensor for the determination of chemical oxygen demand. *Adv. Mater.* **20**, 1044–1049 (2008).
16. Zhang, Z., Zhang, L., Hedhili, M. N., Zhang, H. & Wang, P. Plasmonic gold nanocrystals coupled with photonic crystal seamlessly on TiO_2 nanotube photoelectrodes for efficient visible light photoelectrochemical water splitting. *Nano Lett.* **13**, 14–20 (2013).
17. Lu, X. *et al*. Hydrogenated TiO_2 nanotube arrays for supercapacitors. *Nano Lett.* **12**, 1690–1696 (2012).
18. Zhang, J., Bang, J. H., Tang, C. & Kamat, P. V. Tailored TiO_2–$SrTiO_3$ heterostructure nanotube arrays for improved photoelectrochemical performance. *ACS Nano* **4**, 387–395 (2010).
19. Yuan, L., Meng, S., Zhou, Y. & Yue, Z. Controlled synthesis of anatase TiO_2 nanotube and nanowire arrays via AAO template-based hydrolysis. *J. Mater. Chem. A* **1**, 2552–2557 (2013).
20. Yoo, H. *et al*. Understanding photoluminescence of monodispersed crystalline anatase TiO_2 nanotube arrays. *J. Phys. Chem. C* **118**, 9726–9732 (2014).
21. Li, S., Zhang, G., Guo, D., Yu, L. & Zhang, W. Anodization fabrication of highly ordered TiO_2 nanotubes. *J. Phys. Chem. C* **113**, 12759–12765 (2009).
22. Naito, K., Tachikawa, T., Fujitsuka, M. & Majima, T. Single-molecule observation of photocatalytic reaction in TiO_2 nanotube: importance of molecular transport through porous structures. *J. Am. Chem. Soc.* **131**, 934–936 (2009).
23. Liu, R. & Sen, A. Controlled synthesis of heterogeneous metal-titania nanostructures and their applications. *J. Am. Chem. Soc.* **134**, 17505–17512 (2012).
24. Bavykin, D. V., Passoni, L. & Walsh, F. C. Hierarchical tube-in-tube structures prepared by electrophoretic deposition of nanostructured titanates into a TiO_2 nanotube array. *Chem. Commun.* **49**, 7007–7009 (2013).
25. Xu, X. *et al*. Tube-in-tube TiO_2 nanotubes with porous walls: fabrication, formation mechanism, and photocatalytic properties. *Small* **7**, 445–449 (2011).
26. Li, G., Liu, J. & Jiang, G. Facile synthesis of spiny mesoporous titania tubes with enhanced photocatalytic activity. *Chem. Commun.* **47**, 7443–7445 (2011).
27. Pathakoti, K. *et al*. Photoinactivation of *Escherichia coli* by sulfur-doped and nitrogen–fluorine-codoped TiO_2 nanoparticles under solar simulated light and visible light irradiation. *Environ. Sci. Technol.* **47**, 9988–9996 (2013).
28. Nam, S. H., Kim, T. K. & Boo, J. H. Physical property and photo-catalytic activity of sulfur doped TiO_2 catalysts responding to visible light. *Catal. Today* **185**, 259–262 (2012).
29. Han, C. *et al*. Innovative visible light-activated sulfur doped TiO_2 films for water treatment. *Appl. Catal. B-Environ.* **107**, 77–87 (2011).
30. Rengifo-Herrera, J. A. *et al*. Abatement of organics and Escherichia coli by N, S co-doped TiO_2 under UV and visible light. implications of the formation of singlet oxygen ($^1O_2$) under visible light. *Appl. Catal. B-Environ.* **88**, 398–406 (2009).
31. Dozzi, M. V., Livraghi, S., Giamello, E. & Selli, E. Photocatalytic activity of S- and F-doped TiO_2 in formic acid mineralization. *Photochem. Photobiol. Sci.* **10**, 343–349 (2011).
32. Dong, F., Zhao, W. & Wu, Z. Characterization and photocatalytic activities of C, N and S co-doped TiO_2 with 1D nanostructure prepared by the nano-confinement effect. *Nanotechnology* **19**, 365607 (1–10) (2008).
33. Xu, J. H. *et al*. Simple fabrication of twist-like helix N,S-codoped titania photocatalyst with visible-light response. *Appl. Catal. B-Environ.* **79**, 72–80 (2008).
34. Yu, J. C. *et al*. Efficient visible-light-induced photocatalytic disinfection on sulfur-doped nanocrystalline titania. *Environ. Sci. Technol.* **39**, 1175–1179 (2005).
35. Rockafellow, E. M., Stewart, L. K. & Jenks, W. S. Is sulfur-doped TiO_2 an effective visible light photocatalyst for remediation? *Appl. Catal. B-Environ.* **91**, 554–562 (2009).
36. Nam, S.-H., Kim, T. K. & Boo, J.-H. Physical property and photo-catalytic activity of sulfur doped TiO_2 catalysts responding to visible light. *Catal. Today* **185**, 259–262 (2012).
37. Pelaez, M. *et al*. A review on the visible light active titanium dioxide photocatalysts for environmental applications. *Appl. Catal. B-Environ.* **125**, 331–349 (2012).
38. Asiri, A. M. *et al*. Enhanced visible light photodegradation of water pollutants over N-, S-doped titanium dioxide and n-titanium dioxide in the presence of inorganic anions. *J. Saudi Chem. Soc.* **18**, 155–163 (2014).
39. Marschall, R. & Wang, L. Non-metal doping of transition metal oxides for visible-light photocatalysts. *Catal. Today* **225**, 111–135 (2014).
40. Lee, Y.-C. *et al*. Self-assembled grapheme oxide with organo-building blocks of Fe-aminoclay for heterogeneous Fenton-like reaction at near-neutral pH: a batch experiment. *Appl. Catal. B-Environ.* **142–143**, 494–503 (2013).
41. Lee, Y.-C. *et al*. Oil extraction by aminoparticle-based H_2O_2 activation *via* wet microalgae harvesting. *RSC Adv.* **3**, 12802–12809 (2013).
42. Grätzel, M. Solar energy conversion by dye-sensitized photovoltaic cells. *Inorg. Chem.* **44**, 6841–6851 (2005).
43. Boschloo, G. & Hagfeldt, A. Characteristics of the iodide/triiodide redox mediator in dye-sensitized solar cells. *Accounts Chem. Res.* **42**, 1819–1826 (2009).
44. Lee, J. S., You, K. H. & Park, C. B. Highly photoactive, low bandgap TiO_2 nanoparticles wrapped by grapheme. *Adv. Mater.* **24**, 1084–1088 (2012).
45. Chowdhury, P., Moreira, J., Gomaa, H. & Ray, A. K. Visible-solar-light-driven photocatalytic degradation of phenol with dye-sensitized TiO_2: parametric and kinetic study. *Ind. Eng. Chem. Res.* **51**, 4523–4532 (2012).
46. Lee, H. U. *et al*. Photoluminescent carbon nanotags from harmful cyanobacteria for drug delivery and imaging in cancer cells. *Sci. Rep.* **4**, 4665 (1–7) (2014).

Acknowledgments

This research was supported by the KBSI research Grant No. E34800.

Author contributions

H.U.L., S.C.L., Y.-C.L., Y.-S.L. and J.L. designed the project, organized the entire research. H.U.L., S.C.L., Y.-C.L., S.Y.P., S.C. and J.L. wrote the manuscript. H.U.L., S.C.L., Y.-C.L., J.W.L. and S.Y.P. carried out the sample preparation and characterization. B.S. performed the XPS analysis. Y.K. measured the photocurrents. H.U.L., Y.-C.L., S.Y.P., S.C. and Y.-K.O. performed the photocatalytic activities and cytotoxicity testing of dye purified water by *eco*-TiO_2. All authors discussed the results and commented on the manuscript.

Additional information

Supplementary information accompanies this paper at http://www.nature.com/scientificreports

Competing financial interests: The authors declare no competing financial interests.

How to cite this article: Lee, H.U. *et al*. Innovative three-dimensional (3D) *eco*-TiO_2 photocatalysts for practical environmental and bio-medical applications. *Sci. Rep.* **4**, 6740; DOI:10.1038/srep06740 (2014).